JOURNAL OF Materials CHEMISTRY

Preparation of Y_2O_3-stabilized ZrO_2 thin electrolyte films from Langmuir–Blodgett film precursors by means of "surface ions"

Zou Gang,[a] Fang Kun,[a] He Pingsheng*[a] and Song Haizeng[b]

[a]*Department of Polymer Science and Engineering, Hefei 230026 Anhui, China. E-mail: hpsm@ustc.edu.cn*
[b]*Department of Materials Science and Engineering, University of Science and Technology of China, Hefei 230026 Anhui, China*

Received 22nd March 2002, Accepted 18th May 2002
First published as an Advance Article on the web 9th August 2002

Ultrathin Y_2O_3-stabilized ZrO_2 films have been prepared using Langmuir–Blodgett (LB) films as precursors. The β-diketonate complexes zirconium(IV) 2,2,6,6-tetramethylheptanedionate ($Zr(tmhd)_4$) and yttrium(III) 2,2,6,6-tetramethylheptanedionate ($Y(tmhd)_3$) were chosen as the "surface ions" which can combine with arachidic acid (AA) to form uniform mixed monolayers on pure water. Y-type LB films were fabricated by depositing the mixed monolayers with a mixing ratio of $Y(tmhd)_3/Zr(tmhd)_4/AA = 1:4.5:11$. The YSZ films were obtained through a combination of low temperature ultra-violet/ozone (UVO) decomposition and annealing treatments at high temperature. X-Ray diffraction (XRD) and X-ray photoelectron spectroscopy (XPS) measurements demonstrate that the final films are a single YSZ phase with a fluorite cubic structure and the composition of the films can be well controlled throughout the whole process. Atomic force microscopy (AFM) and cross-section scanning electronic microscopy (SEM) have been employed to reveal the character of the final films.

Introduction

Solid oxide fuel cells (SOFCs) have been considered to be promising energy conversion devices because of their high efficiency and fuel flexibility. Conventional SOFCs with a thick solid electrolyte of Y_2O_3-stabilized ZrO_2 (YSZ) have been limited in commercial applications due to the high operating temperatures required. If the operating temperature could be reduced to less than 800 °C, the advantages of SOFCs such as high efficiency could appear and a variety of usable fuels could be obtained.[1]

Several physical and chemical processes have been employed to prepare thin solid electrolyte films,[2–9] including chemical vapor deposition (CVD), electrophoretic deposition (EPD),[2] electrochemical vapor deposition (EVD),[3,6] plasma spraying,[5] sputtering, metallo-organic chemical vapor deposition (MOCVD),[7–9] dip coating and other wet chemical processes. But there are certain disadvantages in these methods. For example, EVD[6] cannot obtain a dense film.

A Langmuir monolayer is an insoluble amphiphilic layer floating at the air–water interface. A LB film consists of multilayers formed by transferring a highly compressed state sequentially onto a solid support. So the LB process allows for superior control of the thickness and uniformity of the resulting multilayer structure. Recently a new method has been proposed to produce inorganic oxide films starting from a LB film precursor. To our knowledge, most of these works used LB films as precursors for the single oxide, such as ferrous[10] and ferric oxide,[11–14] rare earth oxide,[15–18] Cd oxide,[19] Zn oxide[20] and Ti oxide.[21] All these works employed metal salts in the aqueous subphase. The metal ions were adsorbed onto the monolayer from the subphase by stochastic processes. The technique was successful in producing single component LB films, but it was not easy to obtain multi-component LB films by mixing various metal salts into the aqueous subphase. Although a two-dimensional sol–gel process at the air–water interface was used to fabricate LB films as precursors, it is limited in formation of single oxide thin ceramic films.[22]

Alternatively, we have reported a feasible project in which metal complexes were used as "surface ions" instead of "subphase ions" to form multi-component LB films.[23] This method is developed from one type of "surface ion" to two types of "surface ions" in this presentation. Now $Zr(tmhd)_4$ and $Y(tmhd)_3$ were chosen as the "surface ions" and uniform ultrathin multi-component LB films were obtained. The proposed project is expected to be a promising chemical process for the fabrication of multi-component ceramic nanofilms that can be used as solid electrolyte films in SOFCs.[24,25]

Experimental

The commercially available β-diketonate complexes of $Zr(tmhd)_4$, $Y(tmhd)_3$ (Gelest Inc.) and AA (arachidic acid, spectral purity) were used without further purification. They were dissolved in chloroform solution separately to form solutions with concentrations of 2.11×10^{-3} mol L^{-1}. Both $Zr(tmhd)_4$ and $Y(tmhd)_3$ chloroform solutions were mixed with the AA chloroform solution in a ratio of 1:2 respectively, and the two resulting mixtures were mixed in a ratio of $Y(tmhd)_3/Zr(tmhd)_4/AA = 1:4.5:11$ to obtain the monolayer-forming solution. Pure water (doubly distilled and purified by a quartz sub-boiling ultra purified distiller, pH 5.8) was used as the subphase. The monolayer spreading and LB film deposition were carried out on a homemade computer-controlled Langmuir trough with a Wilhelmy Pt-plate kept in clean room at 25 °C. The monolayers were compressed at a barrier velocity of 8 mm min^{-1} after 30 min spreading. The LB films were deposited with a deposition speed of 2 mm min^{-1} under a constant surface pressure of 35 mN m^{-1}. The substrates used were hydrophobic silicon (100) wafers (modified by adsorbing a single mixed layer of octyldecyltrichlorosilane (OTS) and stearic acid (SA) with a mixing ratio of OTS:SA = 1:2 to improve the deposition process).

LB films were partially decomposed by low temperature ultra-violet/ozone (UVO) decomposition treatment using a low-pressure mercury discharge lamp as the UV light source under an oxygen atmosphere. Ozone gas is produced as a result

 DOI: 10.1039/b202919g

of the reaction of the UV light with oxygen. The UVO decomposition was monitored on a Nicolet MAGNA 750 FTIR spectrometer.

The residual films after UVO treatment were heated in ambient air at a ramp rate of 3 °C min^{-1} up to 650, 850, 1000 and 1100 °C respectively for 3 hours to prepare YSZ films. To characterize the structure of as-deposited LB films and annealed thin films, the XRD profile was recorded on a RIGAKU D/max-γA rotating anode X-ray diffractometer using the Cu-Kα line (λ = 0.15418 nm) with DS = 1°, SS = (1/6)°, RS = 0.15 mm and RS_m = 0.3 mm.The tube current and voltage were 50 mA and 40 kV respectively. The surface morphology of the films after annealing was studied by atomic force microscopy (AFM SPA-300HA) and the thickness of the final films was studied by cross-section scanning electron microscopy (SEM X-650).

Elemental composition and the oxidation of the films were investigated by XPS (VG ESCALAB MK-II photoelectron spectrometer). The vacuum of the analysis chamber was better than 2×10^{-8} Pa. The Mg-Kα radiation ($h\nu$ = 1253.6 eV) was used as an excitation source with the emission current of 20 mA and the anode voltage of 12 kV. The constant analyzer energy of 20 eV was adopted for the spectral data collection. The overall energy resolution was about 1.0 eV under the experimental conditions.

Results and discussion

Monolayer behavior at the air–water interface

Langmuir monolayers usually include gaseous, liquid expanded, liquid condensed and solid states. The π–A isotherms of $Zr(tmhd)_4$, $Y(tmhd)_3$, AA, $Zr(tmhd)_4$/AA, $Y(tmhd)_3$/AA and $Zr(tmhd)_4$/$Y(tmhd)_3$/AA monolayers are shown in Fig. 1. Both $Zr(tmhd)_4$ and $Y(tmhd)_3$ are not hydrophobic enough to form good monolayers on a pure water subphase (Fig. 1a and b) and cannot be used for LB film deposition directly. However, the mixture of $Zr(tmhd)_4$ or $Y(tmhd)_3$ or $Zr(tmhd)_4$/$Y(tmhd)_3$ (Zr : Y = 4.5 : 1) with AA (mixing ratio is 1 : 2) can form a uniform monolayer on pure water (Fig. 1c, d and e). Compared with the AA monolayer (Fig. 1f), the mixed monolayer has no liquid state and exhibits high compressibility due to the strong combining force among the molecules in plane. UV-vis spectral analyses show that the chloroform solutions of $Zr(tmhd)_4$ and $Y(tmhd)_3$ have absorption edges at 363 and 393 nm, which are shifted to 326 and 322 nm respectively when AA is mixed in (Fig. 2). These results clearly show that AA molecules are combined with $Zr(tmhd)_4$ or $Y(tmhd)_3$ as new ligands. All the information suggests that there must be some combining forces occurring between AA and $Zr(tmhd)_4$ or $Y(tmhd)_3$ due to the big difference in electro negativity between oxygen and

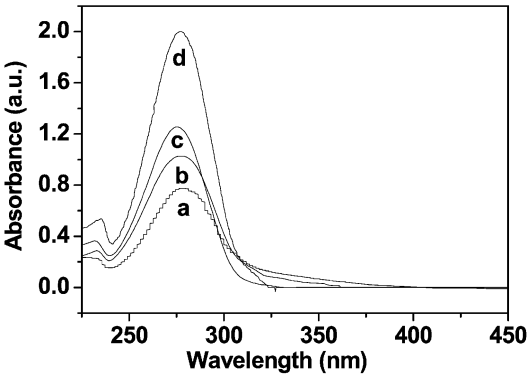

Fig. 2 The UV-visible absorption spectra of chloroform solutions of $Zr(tmhd)_4$ **(a)**, $Y(tmhd)_3$ **(b)**, $Zr(tmhd)_4$/AA = 1 : 2 **(c)** and $Y(tmhd)_3$/AA = 1 : 2 **(d)**.

zirconium or yttrium. The combined molecules, $Zr(tmhd)_4$–AA or $Y(tmhd)_3$–AA, are hydrophobic enough to form a good monolayer on the pure water subphase and can be used for LB film deposition.

LB film formation

In general, LB films have poor mechanical properties for direct applications and can be easily destroyed. In this experiment, the substrates were treated with OTS/SA in order to improve the layers' adhesion to substrate. The mixed monolayer with a mixing ratio of $Y(tmhd)_3$/$Zr(tmhd)_4$/AA = 1 : 4.5 : 11 can be transferred onto hydrophobic silicon (100) wafers, by both downward and upward strokes under a constant surface pressure of 35 mN m^{-1} with a transfer ratio of unity. The dry time for every deposited layer is 15 minutes. Multi-component Y-type mixed LB films were obtained and the LB film looks uniform and plain. XRD studies indicated that the preparation of the LB films was successful. Fig. 3 shows the low angle X-ray diffraction profiles of a 400-layer $Zr(tmhd)_4$–$Y(tmhd)_3$–AA LB film on a silicon wafer. It was evident that the appearance of four equidistant Bragg diffraction peaks in the range of 2θ = 2–10 ° indicated the presence of a regular periodic structure in the $Zr(tmhd)_4$–$Y(tmhd)_3$–AA LB film. Since we concluded earlier that $Zr(tmhd)_4$ and $Y(tmhd)_3$ are incorporated in the multilayers, the "surface ions" of $Zr(tmhd)_4$ and $Y(tmhd)_3$ would be expected to act as efficient scattering centers. Assigning (001), (002)···(00l) to the Bragg peaks in Fig. 3 from left to right, the spacing in the LB films can be expressed as $d = ld_{00l}$. From this equation, we calculated the average spacing of the LB films to be d = 5.56 nm. It should be noted that the first Bragg peak was in the very low angle (2θ = 1.6°), and the detector of the X-ray diffractometer almost received the incident light with a reflecting angle close to the critical

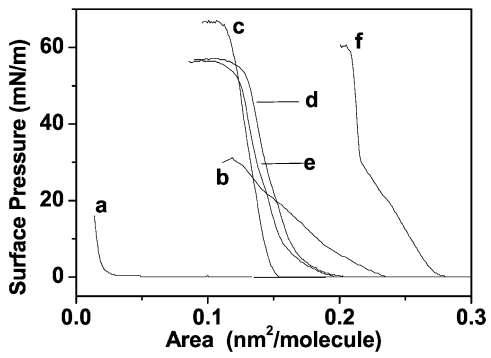

Fig. 1 π–A curves of pure $Y(tmhd)_3$ **(a)**, pure $Zr(tmhd)_4$ **(b)**, $Y(tmhd)_3$/AA = 1 : 2 **(c)**, $Zr(tmhd)_4$/AA = 1 : 2 **(d)**, $Y(tmhd)_3$/$Zr(tmhd)_4$/AA = 1 : 4.5 : 11 **(e)** and pure AA **(f)** on pure water.

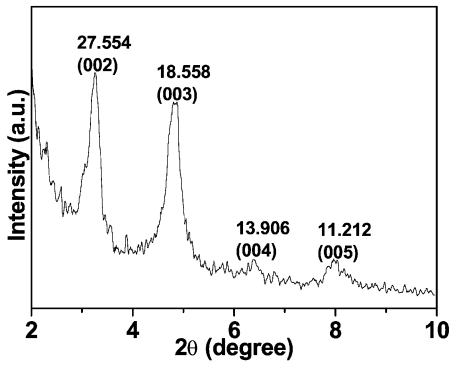

Fig. 3 X-Ray diffraction profiles from the 400 layers of a mixed LB film with a mixing ratio of $Y(tmhd)_3$/$Zr(tmhd)_4$/AA = 1 : 4.5 : 11 on a hydrophobic silicon (100) wafer.

angle ($2\theta = 1°$ for the instrument here) of total reflection. For this reason the value of the first peak was omitted in our calculation of the average *d*-value. The Bragg reflections of the mixed LB films greatly reduced in peak intensity and sharpness compared with what is seen from the well-known fatty acid salt multilayers of comparable thickness. This is mainly because of the bulky size of $Zr(tmhd)_4$ and $Y(tmhd)_3$ or local failure of deposition of the mixed LB films. However, what is important is that the 400-layer mixed LB films with a thickness of about 1.11 μm are uniform enough for the fabrication of ceramic YSZ films.

UVO decomposition of the LB precursors

The low-temperature UVO technique proved to be the key step in bypassing the film's melting non-uniformity.[15] The UVO decomposition was monitored by FTIR analysis (Fig. 4) through the disappearance of the C–H modes and the $–CO_2^-$ bond (vibration originating from the precursor with $\nu(CH_x)$ at 2960–2850 cm^{-1}, $\delta(CH_x)$ at 1470–1430 cm^{-1}, and $\nu(C{=}O)$ at 1548 cm^{-1}). Hydrocarbons in the LB film precursors were almost destroyed after a 12 h UVO process.

Annealing and characterization

The residual films after UVO treatment were heated in ambient air at a ramp rate of 3 °C min^{-1} up to 650, 850, 1000 and 1100 °C for 3 hours. The organic LB films were turned into inorganic oxide thin films and the mechanical properties and adhesion to substrate of the layers were both markedly improved and the films looked quite uniform and plain. XRD measurements were performed to obtain information on the film structure. Four samples were obtained with different annealing processes (shown in Fig. 5). When the film was heated up to 650 °C, it began to form a cubic structure but the diffraction peak was wide and the intensity low which indicates that the film did not form a perfect crystal and the size of the crystalline particles is very small. The higher the annealing temperature, the narrower and higher are the corresponding XRD peaks. According to the Scherrer equation, the crystal size of the individual grains should be relatively big with increasing annealing temperature. The average crystal size in the residual films annealed at 1000 °C is calculated to be 17.2 nm (average of peak (111) and (200)) using the Scherrer equation. When the films are heated above 1000 °C, the residual films are indeed a single YSZ phase with a fluorite cubic structure and there is no other phase structure. By comparison with the data of the standard XRD profile, it can also be found that the intensity of the (200) peak is seen to increase, apparently without observable change in position. This suggests that the high temperature will increase the rate of crystallization and result in preferred orientation of the individual grains.

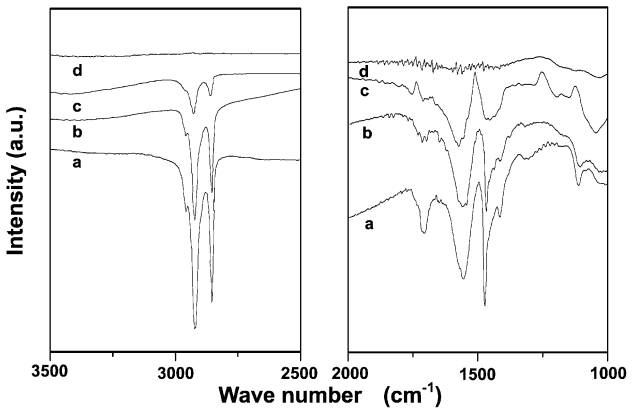

Fig. 4 FTIR spectra of 400 layers of $Y(tmhd)_3/Zr(tmhd)_4/AA$ = 1 : 4.5 : 11 on hydrophobic silicon (100) wafers with respect to UVO processing time: **(a)**, as-deposited; **(b)**, UVO 3 hours; **(c)**, UVO 7.5 hours; **(d)**, UVO 12 hours.

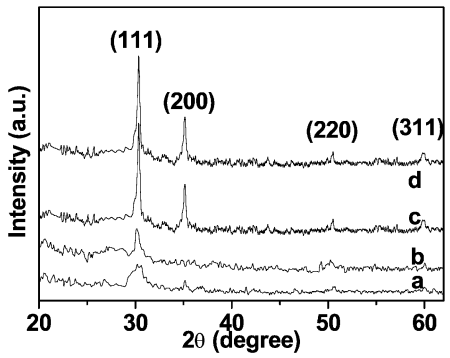

Fig. 5 X-Ray diffraction pattern of ZrO_2 and **(a)** diffraction pattern of a YSZ ceramic film after annealing in air at 650 °C; **(b)**, after annealing in air at 850 °C; **(c)**, after annealing in air at 1000 °C; **(d)**, after annealing in air at 1100 °C.

AFM and SEM measurements were performed to obtain information on the microstructure of the as-produced films. AFM studies have revealed the close molecular packing of the films fired at 1000 °C (Fig. 6a). The fired film looks uniform except that some pinhole disfigurements have been introduced. These disfigurements must be introduced during the annealing process of the final films because the rate of crystallization is very fast at high annealing temperature and it would make the films shrink in plane and produce local disfigurements. The size of the particulates is about 30–40 nm, larger than the crystal size calculated using the Scherrer equation. The existence of disfigurements may broaden the diffraction peak and decrease the crystal size calculated. From the cross-section SEM images of the fired films (Fig. 6b), we can calculate that the thickness of the films is about 1 μm.

XPS measurements were performed to obtain information on the film structure and composition. The sample fired at 1000 °C was chosen for comparison with the as-deposited film and the film just after the UVO process. Fig. 7 is the XPS spectrum of C 1s. For the as-deposited film the peak at 284.8 eV is mainly assigned to hydrocarbon and a small peak at 289.3 eV comes from $–CO_2H$ (Fig. 7a). After UVO treatment the hydrocarbon component is eliminated from the film while $–CO_2H$ still exists (Fig. 7b). The peak at 284.4 eV belongs to adsorbed carbon which is partially removed by UVO exposure so that the peak at 289.3 eV becomes relatively strong. The main reason is possibly that some adsorbed carbons has reacted with the oxide films and formed a carbonate complex. This result is in accordance with the FTIR experiment. After the residual film was annealed in air up to 1000 °C for 3 hours, the peak for $–CO_2H$ at 289.3 eV disappeared (Fig. 7c) while the peak at 284.4 eV for adsorbed carbon remained. This fact suggests that the final film has turned into an inorganic film.

XPS spectra of the O 1s core level in Fig. 8 show dramatic evolution through the three stages. The O 1s peak in Fig. 8 with a binding energy of about 529.5 eV is mainly assigned to the oxide and the one at 531.8 eV comes from either adsorbed oxygen or oxygen remaining in the film. UVO exposure partially enhanced the former peak (Fig. 8b) which indicates that the oxygen assigned to the oxide increased. As seen in Fig. 8c, the intensity of the peak at 529.5 eV becomes stronger, almost equal to the one at 531.8 eV after annealing. All these results indicate that the final film has turned into an inorganic oxide film.

The Zr 3d core level spectra are displayed in Fig. 9.There are only two peaks in the as-deposited LB films (Fig. 9a). They both belong to zirconium and these two peaks shift to the left in the UVO treated film (Fig. 9b). And the intensities of these two peaks are both enhanced. The reason is that UVO exposure

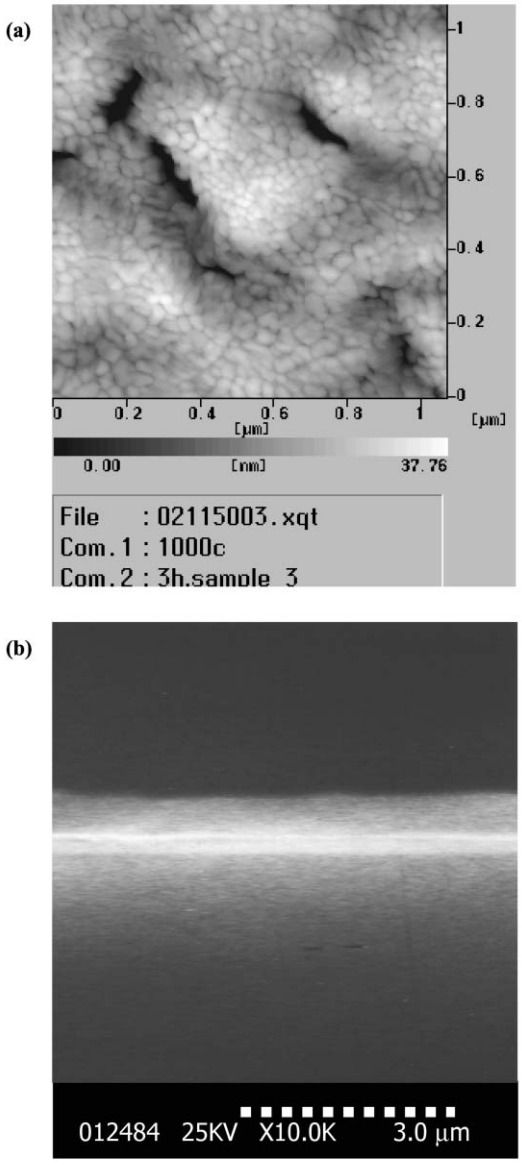

Fig. 6 AFM images of the YSZ ceramic films after annealing in air at 1000 °C for 3 hours **(a)** and the cross-section SEM images of the YSZ ceramic films after annealing in air at 1000 °C for 3 hours **(b)**.

partially removes the carbon of the films so that the content of zirconium seems relatively higher. After annealing treatment these two peaks continue to shift to the left and turns out to

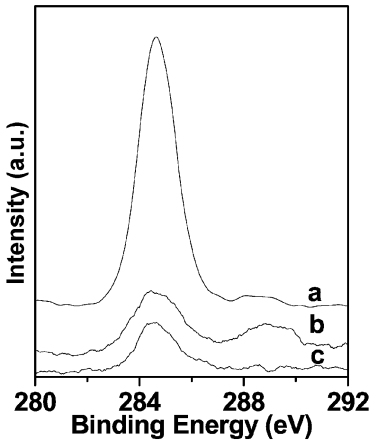

Fig. 7 (a) The XPS spectra of C 1s from the LB precursor, **(b)** residual film after UVO treatment, and **(c)** YSZ ceramic film after annealing in air at 1000 °C for 3 hours.

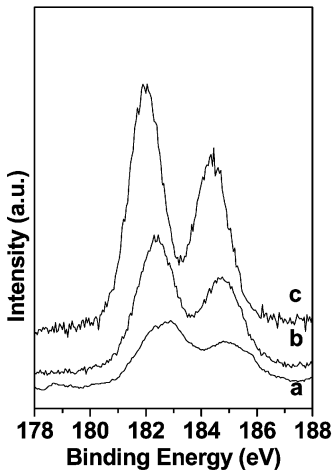

Fig. 9 (a) The Zr 3d XPS spectra from the LB precursor; **(b)** residual film after UVO treatment for 24 hours; **(c)** YSZ ceramic film after annealing in air at 1000 °C for 3 hours.

both belong to ZrO_2. We should note that the binding energy of the zirconium complex in LB films is slightly smaller than that of the zirconium oxide in ceramic nanofilms. Comparing with the results of the XRD profile, we can see that the final films have already changed into ZrO_2 ceramic nanofilms with a fluorite cubic structure.

XPS spectra of the Y 3d core level are displayed in Fig. 10.

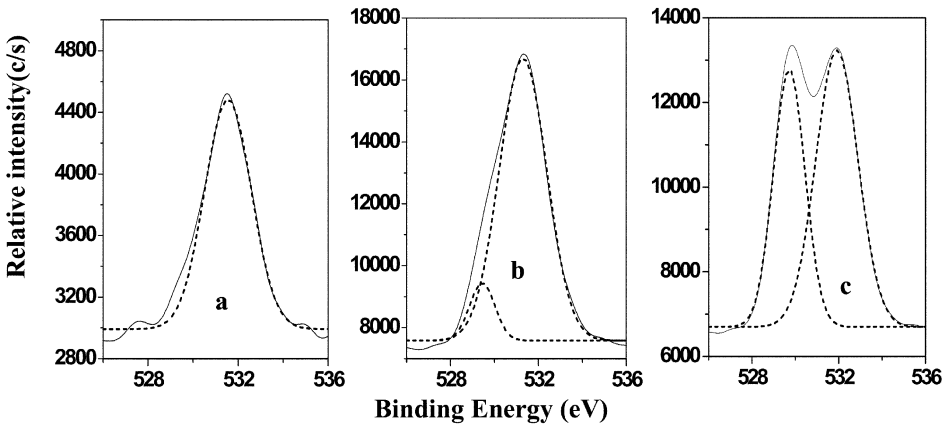

Fig. 8 (a) The XPS spectra of O 1s from the LB precursor, **(b)** residual film after UVO treatment, and **(c)** YSZ ceramic film after annealing in air at 1000 °C for 3 hours.

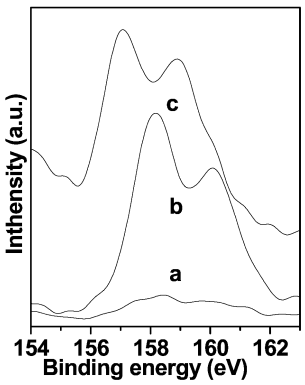

Fig. 10 **(a)** The Y 3d XPS spectra from the LB precursor; **(b)** residual film after UVO treatment for 24 hours; **(c)** YSZ ceramic film after annealing in air at 1000 °C for 3 hours.

Table 1 The composition of the films

	C (%)	O (%)	Zr (%)	Y (%)	Zr : Y	Relative error (%)
a. As-deposited film	88.6	9.3	1.7	0.4	4.3 : 1	10
b. Residual film after UVO	25.5	56.3	14.8	3.4	4.4 : 1	10
c. YSZ film after annealing	7.3	73.4	15.7	3.6	4.4 : 1	10

There are only two peaks in the as-deposited LB films (Fig. 10a). Because the content of yttrium is very low, the XPS analysis can only prove the existence of yttrium, but cannot give an accurate yttrium content. These two peaks shift to the left in the UVO treated film and the intensities of these two peaks are both enhanced (Fig. 10b). The reason is that UVO exposure partially removes the carbon of the films so that the content of zirconium appears higher. XPS analysis can not only prove the existence of yttrium, but also give the accurate content of yttrium. After annealing treatment these two peaks continually shift to the left (Fig. 10c) and the result proves that yttrium has turned into Y_2O_3 doped in ultrathin ceramic nanofilms.

The compositions of the samples after passing through the three stages (as-deposited, after UVO treatment and after annealing) are listed in Table 1. We can obtain the composition of the samples in XPS analysis by comparing the spectral intensity of every element at each stage. According to the results, the surface of the fired film contains mainly C, O, Zr and Y. Passing through the three stages, the content of C decreases substantially while the content of O increases. In the first stage, XPS analysis cannot give the accurate content of yttrium due to the low content of yttrium in the as-deposited films and the Zr : Y ratio is also not very accurate. But the Zr : Y ratio remained the same during the last two stages. The final result is a little lower than that of the mixing ratio. This is mainly caused by the deposition process of the LB films. All the results prove that the composition of the film can be controlled throughout the whole process. In this work the Zr : Y ratio (4.5 : 1) is used to illustrate that the composition of the film can be controlled, although it is not the most suitable ratio (7–8 mol%) generally accepted for practical applications in SOFCs and the Zr : Y ratio in the final oxide films can be easily adjusted by changing the mixing ratio of the mixed monolayer. This offers us a new method to fabricate component controllable YSZ films.

Conclusion

Metal complexes, $Zr(tmhd)_4$ and $Y(tmhd)_3$, were used as " surface ions" and incorporated into a AA monolayer on pure water to form multi-component mixed LB precursors successfully. UVO treatment is employed to suppress the droplet formation during heating. The residual films after UVO treatment were heated to form YSZ ceramic films. XRD and XPS indicate that the fired films are a single YSZ phase with a fluorite cubic structure. The annealing temperature affects the average size of grains and morphology of the film. In this work we demonstrate a promising method to fabricate component-controllable ceramic nanofilms. This method can be extended to multi-component ceramic films formation and applied to form not only solid electrolyte films but also super-conducting films, giant magnetic resistance film and so on.

Acknowledgements

This work is supported by the National Nature Science Foundation of China (29974028).

References

1 N. Q. Minh, *J. Am. Ceram. Soc.*, 1993, **76**(3), 563–588.
2 T. Ishihara, K. Sato and Y. Takita, *J. Am. Ceram. Soc.*, 1996, **79**(4), 913–919.
3 U. B. Pal and S. C. Singhal, *J. Electrochem. Soc.*, 1990, **137**(9), 2937–2941.
4 S. De Souza, S. J. Visco and L. C. De Jonghe, *Solid State Ionics*, 1997, **98**(1–2), 57–61.
5 A. R. Nicoll, A. Salito and K. Honegger, *Solid State Ionics*, 1992, **52**(1–3), 269–275.
6 J. Han, Y. Zeng, G. Xomeritalis and Y. S. Lin, *Solid State Ionics*, 1997, **98**(1–2), 63–72.
7 M. Pan, G. Y. Meng, H. W. Xin, C. S. Chen, D. K. Peng and Y. S. Lin, *Thin Solid Films*, 1998, **324**(1–2), 89–93.
8 G. Garcia, J. Casado, J. Llibre and A. Figueras, *J. Cryst. Growth*, 1995, **56**(4), 426–432.
9 G. Garcia, A. Figueras, J. Casado, J. Llibre, M. Mokchah, G. Petot-Ervas and J. Calderer, *Thin Solid Films*, 1998, **317**(1–2), 241–244.
10 Y. Ando, T. Hiroike, T. Miyashita and T. Miyazaki, *Thin Solid Films*, 1995, **266**(2), 292–297.
11 T. Tippmann-Krayer, W. Meisel, U. Hohne and H. Mohwald, *Makromol. Chem., Macromol. Symp.*, 1991, **46**, 241–246.
12 T. Faldum, W. Meisel and P. Güitlich, *Surf. Interface Anal.*, 1996, **24**(1), 68–73.
13 T. Faldum, W. Meisel and P. Güitlich, *Hyperfine Interact.*, 1994, **92**(1–4), 1263–1269.
14 D. Brandl, Ch. Schoppmann, Ch. Tomaschko, J. Markl and H. Voit, *Thin Solid Films*, 1994, **249**(1), 113–117.
15 D. T. Amm, D. J. Johnson, T. Laursen and S. K. Gupta, *Appl. Phys. Lett.*, 1992, **61**(5), 522–524.
16 T. Laursen, G. R. Palmer, D. T. Amm and D. Johnson, *Nucl. Instrum. Methods Phys. Res., Sect. B*, 1993, **82**(1), 125–128.
17 M. Schurr, J. Hassmann, R. Kügler, C. Tomaschko and H. Voit, *Thin Solid Films*, 1997, **307**(1–2), 260–265.
18 D. T. Amm, D. J. Johnson, N. Matsuura, T. Laursen and G. Palmer, *Thin Solid Films*, 1994, **242**(1–2), 74–77.
19 N. Matsuura, D. J. Johnson and D. T. Amm, *Thin Solid Films*, 1997, **295**(1–2), 260–265.
20 D. M. Taylor and J. N. Lambi, *Thin Solid Films*, 1994, **243**(1–2), 384–388.
21 D. V. Paranjape, M. Sastry and P. Ganguly, *Appl. Phys. Lett.*, 1993, **63**(1), 18–20.
22 M. Oswald, V. Hessel and R. Riedel, *Thin Solid Films*, 1999, **339**(1–2), 284–289.
23 W. X. Lu, W. H. Guo, H. L. Zhou and P. S. He, *Langmuir*, 2000, **16**(11), 5137–5141.
24 J. P. P. Huijsmans, F. P. F. van Berkel and G. M. Christie, *J. Power Sources*, 1998, **71**(1–2), 107–110.
25 W. X. Lu, K. Fang, W. H. Guo, P. S. He and M. L. Ji, *Thin Solid Films*, 2002, in press.